Equiaxed grain structure formation during directional solidification of a refined Al-20wt.%Cu alloy: in situ analysis of temperature gradient effects

H. Soltani, G. Reinhart, M.C. Benoudia, F. Ngomesse, M. Zahzouh, H. Nguyen-Thi

Equiaxed grain structure formation during directional solidification of a refined Al-20wt.%Cu alloy: *in situ* analysis of temperature gradient effects

H. Soltani[b], G. Reinhart[a,*], M. C. Benoudia[c], F. Ngomesse[a], M. Zahzouh[b], H. Nguyen-Thi[a]

[a] Aix Marseille Univ, Université de Toulon, CNRS, IM2NP, Marseille, France

[b] Badji Mokhtar University, LMGM, BP 12, 23000, Annaba, Algeria

[c] Ecole Nationale Supérieure des Mines et de la Métallurgie, L3M, Annaba, Algeria

Abstract

Three series of directional solidification experiments on refined Al-20wt.%Cu alloys have been carried out with different temperature gradients, and for each of them a wide range of cooling rates were applied. The experiments were performed in horizontal configuration to minimize the impact of gravity-driven phenomena and characterized *in situ* and in real-time by using the X-radiography technique. The influence of the temperature gradient on the microstructure formation (impact of Temperature Gradient Zone Melting: TGZM), the nucleation distance, the

* Corresponding author at Aix-Marseille University and IM2NP Case 142, Campus St-Jerome, 13397 Marseille cedex 20, France: Tel.: (+33) 4 91 28 28 94; Email address: guillaume.reinhart@im2np.fr

average grain size and morphology (elongation factor and grain orientation) have been analysed quantitatively. The experimental results are discussed with current theoretical models and similar experimental works.

Keywords: A1. Directional solidification, A1. Characterization; A1. Dendrites; A1. Nucleation; B1. Alloys; B1. Metals

1. Introduction

In most industrial solidification processes, equiaxed grain structures are required because they give uniform and isotropic properties to the final product, unlike columnar grain structures. The size and the morphologies of the grains affect the segregation distribution and therefore the final mechanical and chemical properties of materials [1, 2]. Numerous studies have been undertaken to understand the relationships between grain characteristics and the variation of solidification parameters such as alloy composition, temperature gradient and growth velocity or cooling rate. However, the genesis of dendritic grains from the liquid phase remains a complex multiscale topic, involving several dynamic phenomena (nucleation, diffusion, interaction between grains, fluid flow, buoyancy forces...) whose length and time scales extend over several orders of magnitude and that interact with each other [3].

Most of existing models studied the case of the nucleation and the growth of grains in an isothermal melt, but this condition is hardly achieved in real casting conditions [3, 4]. Moreover,

only some experimental studies tackled the analysis of the equiaxed grain structure formation in the presence of a temperature gradient, which is the most frequent case. Grain refinement of directionally solidified Al–4.15wt.%Mg was studied using a wide range of pulling velocities by Vandyoussefi and Greer [5], who performed experimental observations of elongated grains by post-mortem analyses. A similar research on the cooling rate (or growth velocity) effects on the final grain size was recently carried out by H. Soltani *et al.* [6] using X-radiography during a directional solidification of refined Al-20wt.%Cu alloys in an horizontal configuration. Xu *et al.* [7] investigated the impact of the temperature gradient and proposed a model that quantitatively addresses its effect on the grain nucleation in the liquid phase surrounding the growing grains, extending the work of Jia *et al.* [8] who used synchrotron X-radiography to study the impact of a solute suppressed nucleation zone (SSNZ) on the grain nucleation during the downward solidification of Al-15wt.%Cu alloys.

To observe *in situ* and in real time the dynamic of microstructure formation during the solidification of metal alloys, a great number of experimental works have used X-radiography as an observation technique that gives a 2D projected image. Currently, X-radiography can be done either by using a synchrotron source [9, 10] or with a microfocus laboratory source [11, 12]. The former is very attractive as there is a straightforward relationship between grey level in the radiograph and the composition variations in the sample when using a monochromatic beam [13, 14]. The main drawback is that, due to the horizontal nature of synchrotron beam, only vertical solidification experiments can be carried out, when strong impact of gravity are

expected. This issue is critical for the study of equiaxed grain formation because gravity effects such as natural convection and buoyancy could prevent to draw clear conclusions from the experimental observations. However, in the case of laboratory apparatuses, it is possible to perform solidification in an horizontal configuration where the gravity effects are drastically damped [6, 15]. It is worth to mention that experimentation in microgravity conditions is an irreplaceable way to simplify the solidification process analysis by efficiently eliminating gravity effects, namely natural convection, and buoyancy force, allowing the formation of solidification microstructures to be studied in near-diffusive conditions [16, 17].

In this paper, we focus on the analysis of the temperature gradient effect on the grain structure evolution and its final characteristics during horizontal directional solidification of an Al-20wt.%Cu alloy refined with 0.1wt.% Al-Ti-B. This work completes a previous one that was devoted to studying the impact of cooling rate (or growth velocity) on the grain structure formation [6]. Quantitative analysis of the experiments has been performed based on *in situ* visualisation of the solidification front propagation. The results allowed us to highlight the effect of the temperature gradient on dynamic phenomena taking place during solidification such as the nucleation and growth of new grains, the occurrence of TGZM (Temperature Gradient Zone Melting) and then on the characteristics of the final grain structure (grain size, elongation and growth orientation).

2. Experiments

2.1. SFINX apparatus

Experiments were performed using a microfocus X-radiography device entitled SFINX (Solidification Furnace with IN situ X-radiography) dedicated to the study of the solidification of aluminium-based alloys. A detailed description of the apparatus can be found in [6, 11] and the main experimental details are summarised in the following. The SFINX furnace is an assembly of two identical heating elements, spaced apart by a 5 mm × 5 mm square window defining the field of view (FoV) and enabling X-rays to go through the sample with minimal attenuation. This furnace allows directional solidification to be achieved with applied temperature gradients G between 2.5 K/mm and 15 K/mm, and cooling rates R between 0.01 K/s and 1.5 K/s.

Here, three Al-20wt.%Cu alloys samples refined with 0.1 wt.%Al-Ti-B have been prepared to carry out *in situ* X-radiography experiments. The samples had a main rectangular surface of 50 mm × 5 mm with a thickness of about 200 µm. Each sample was fixed in the middle of stainless-steel spacers sandwiched between two sheets of flexible glassy carbon sewn together with a silica thread. The crucible-sample set was inserted inside the furnace, in direct contact with the two heaters to apply a temperature gradient along the sample. The two heating elements were controlled by two K-type thermocouples positioned 13.5 mm apart from each other. By monitoring separately the respective temperatures of the hot and cold heaters, it was thus possible to adjust the temperature gradient inside the sample. The sample was solidified by

applying the same cooling rate R on both furnace heaters (power-down method) and keeping constant the applied temperature gradient along the whole solidification experiment.

2.2. Solidification experiment parameters

In this paper, three series of experiments were carried out with different applied temperature gradients between the two heaters. For each value of the applied temperature gradient, a series of melting and solidification of the sample with different cooling rates was performed. A reference experiment with a cooling rate of 0.15 K/s was repeated three times to check the repeatability of the observations, and similar distributions of grain size, elongation factor and growth orientation were obtained [6].

For every experiment, the solidification parameters (mean nucleation front velocity V_{mean} and mean temperature gradient G_{mean}) were determined by an analysis of recorded radiographs, as explained in details in [6]. In a first step, the nucleation front velocity is accurately measured along the FoV and a mean value V_{mean} was then deduced. In a second step, the actual mean temperature gradient in the sample G_{mean} was deduced by assuming the relation $G_{mean} = R/V_{mean}$, with R the imposed cooling rate. The values given by this procedure are summarized in Table 1 for all experiments and represented in a (V, G) diagram in Fig.1. The series labelled A, B and C corresponds to experiments carried out with a temperature gradient in the range 3.6 ± 0.6 K/mm, 5.6 ± 0.5 K/mm and 9.4 ± 0.1 K/mm respectively.

Experiments	V_{mean} (µm/s)	G_{mean} (K/mm)
A1	15.5	3.2
A2	30.5	3.3
A3-1; A3-2; A3-3	44; 46; 37.5	3.4; 3.3; 4
A4	83.1	3.6
A5	122	3.7
A6	213	4.2
B1	19.3	5.2
B2-1; B2-2; B2-3	24.5; 25.4; 28.9	6.1; 5.9; 5.2
B3	55.7	5.4
B4	80	5.6
B6	224	6
C1-1; C1-2; C1-3	14.7; 15.6; 15.7	10.2; 9.6; 9.6
C2	32.2	9.3
C3	47.3	9.5
C4	96.3	9.3
C5	142	9.5

Table 1. Solidification parameters of experiments presented in this paper: mean nucleation front velocities and mean temperature gradients (refined Al-20wt.%Cu).

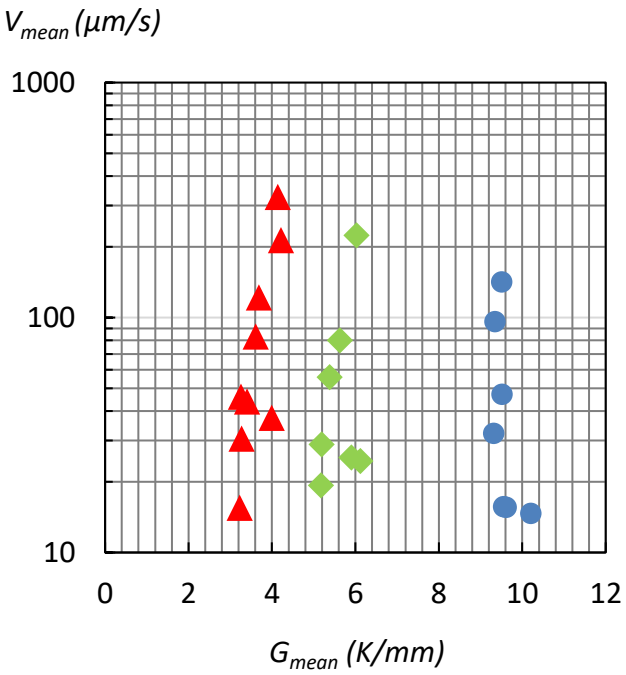

Fig. 1: (V, G) diagram showing the three series of experiments carried out for different applied temperature gradients.

2.3. X-radiography device

The X-radiography system involved an X-ray micro-focus source (3 µm focal spot) with a molybdenum target that generated a photon flux with two peaks of energy at 17.4 keV and 19.6 keV. The X-ray beam divergence induced a geometric magnification of the object on the detector (Fig.2). The magnification was approximately 5, resulting in an effective pixel size of around 4 µm × 4 µm. The acquisition rate was set to 2 frames per second.

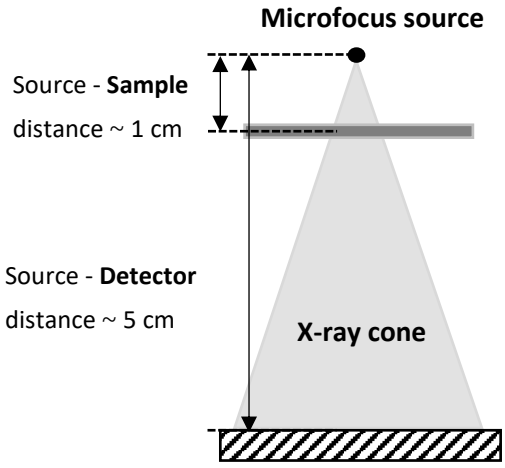

Fig 2: Schematic side view of the furnace showing the X-ray cone passing through the sample and the geometric magnification effect.

The X-ray system records and stores raw images whose variation in grey level depends on the difference in X-ray absorption of each part of the sample. The recorded radiographs were improved by using "*flat-field*" image processing that provides a contrast-enhanced image by removing detector and crucible defects [18]. In the images, the bright regions correspond to the Al-grains surrounded by dark areas of Cu-rich liquid.

2.4. Grain structure characterisation

A semi-automatic macro script was implemented in the software ImageJ [19] to determine the following grain structure characteristics: distribution of grain size, elongation factor and growth orientation as a function of the growth velocity [7] and temperature gradient. The execution of the script required to first draw manually the boundaries of all grains. Then, the grain size defined as the diameter d of the equivalent disk, the elongation factor $\phi = L_1/L_2$ with

L_1 the length of the longest axis contained in the grains and L_2 the length of the longest perpendicular axis, and the growth orientation characterised by θ the angle between the grain main axis and the temperature gradient direction were determined automatically. Additional details about this procedure can be found in [6].

3. Results and discussion

3.1. Transition from equiaxed to columnar grain structure at low growth velocity.

Figure 3 shows the solidification microstructures of experiments A1, B1 and C1-3, which were performed at roughly the same low growth velocity (V_{mean} = 15.5 µm/s, 19.3 µm/s and 15.7 µm/s), and for increasing temperature gradients (G_{mean} = 3.2 K/mm, 5.2 K/mm and 9.6 K/mm). It can be seen from the radiographs that the increase of temperature gradient induces a gradual transition from a roughly equiaxed or slightly elongated grain structure at low temperature gradient (Fig. 3a) to a columnar-grain structure (Fig. 3c). The microstructure with the intermediate temperature gradient consists of a mixing of short and elongated grains (the white area in Fig. 3b at the top of the FoV is due to a slight thinning of the sample, accentuated by image processing). This transition from an equiaxed structure to a columnar structure with the temperature gradient increase agrees to the predictions of Hunt's model [20], which states that at low growth velocity the structure becomes more columnar when temperature gradient is increased. Moreover, the grain structure at high temperature gradient seems more compact, with less liquid between the neighbouring grains. The latter observation can be made for all

experiments performed with roughly the same growth velocity and varying temperature gradient. This observation will be discussed in section 3.3.

Interestingly, for both experiments B1 and C1-3, very long isolated columnar grains were visible, that were able to cross almost the whole FoV (Fig. 3b and Fig. 3c). Such long columnar grains developing through the other grains have been reported in a previous paper [6] and also observed during Al-7wt%Si solidification in cylindrical samples under microgravity conditions on board of the ISS (International Space Station) [21]. The existence of such rare grains was attributed to the better alignment of the columnar dendrite axis with the temperature gradient, that favoured its development with respect to the less well oriented equiaxed grains.

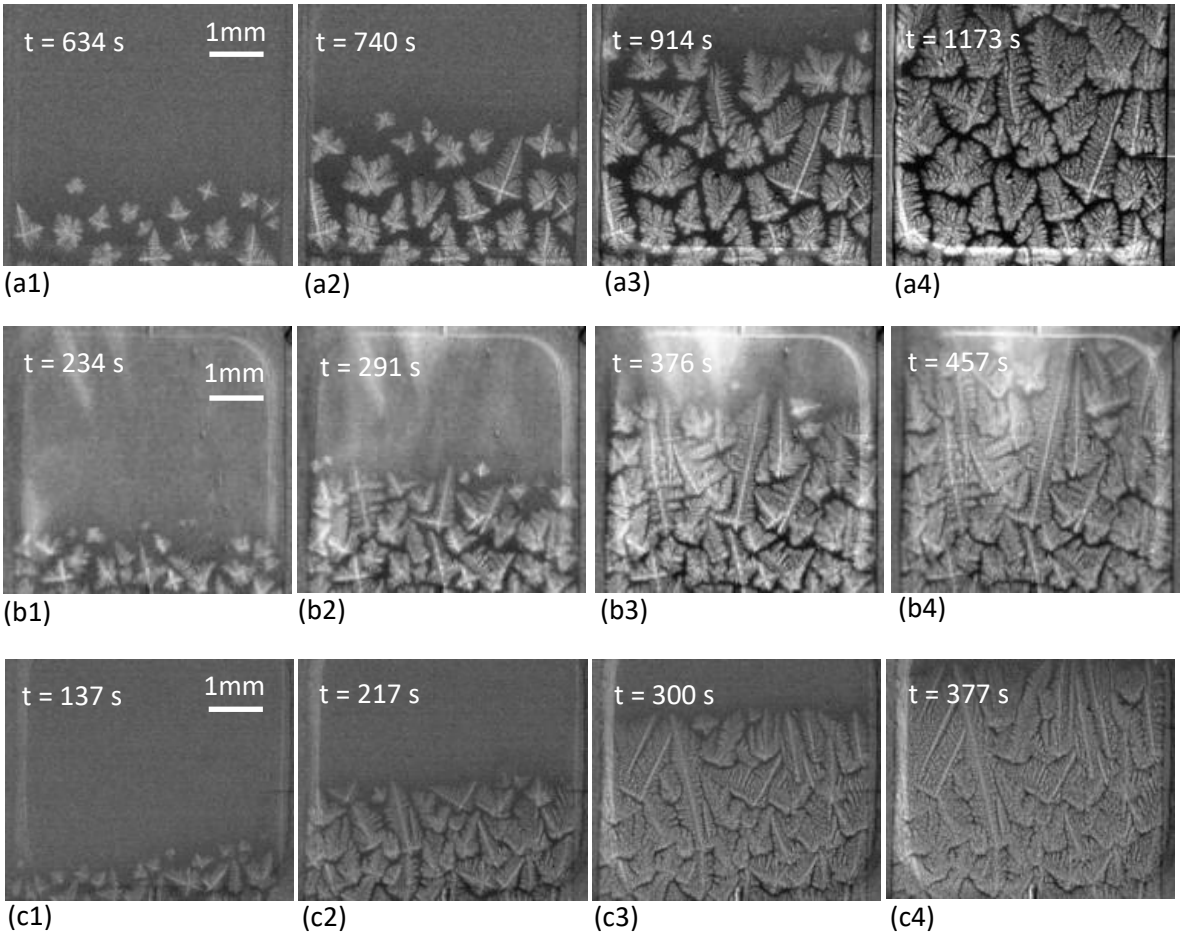

Fig.3: Series of radiographs showing the solidification front propagation and the microstructure variation of the experiments carried out with: (a) Experiment A1 (V_{mean} = 15.5 µm/s and G_{mean} = 3.2 K/mm); (b) Experiment B1 (V_{mean} = 19.3 µm/s and G_{mean} = 5.2 K/mm) and (c) Experiment C1-3 (V_{mean} = 15.7 µm/s and G_{mean} = 9.6 K/mm).

3.2. Influence of TGZM phenomenon at intermediate growth velocity

Figure 4 shows the propagation of the equiaxed fronts through the FoV for another set of three experiments (A2, B2-2 and C2) with nearly the same growth velocities (V_{mean} = 30.5 µm/s, 25.4 µm/s and 32.2 µm/s) and increasing temperature gradients (G_{mean} = 3.3 K/mm; 5.9 K/mm and 9.3 K/mm). At these velocities, the three microstructures are of equiaxed-type. As described in [6, 22], the solidification front propagated by wave-like nucleation ahead of the solidification front, in a similar way to the observations reported by many authors [7, 8, 23, 24]. No buoyancy-driven grain motion was observed in these series of radiographs since the experiments were performed in a horizontal configuration [22]. The entire solidification process of these experiments can be seen in the supplementary videos.

Interestingly, a slow and steady motion toward the hot part of the furnace of all the grains in the mushy zone can be noted when watching the videos. This feature is observed for all experiments and is in fact due to the TGZM (Temperature Gradient Zone Melting) phenomenon, which induces a global migration of all liquid inclusions toward the hot region when a temperature gradient is applied [25, 26]. From the sequences of radiographs, it is possible to determine an average grain migration velocity for the three experiments carried out with different temperature gradients. The procedure is tedious and time-consuming, so that only a

limited number of measurements (about ten grains) were performed for each experiment. The experimental values and their dispersion are reported in Fig.5 and compared to the predicted linear variation given by the simple model of Tiller *et al.* [27]:

$$V_{mig} = \frac{-GD}{mC_L(1-k)} \quad (1)$$

With G the temperature gradient within the liquid channel between the grains, assumed equal to the temperature gradient of the experiment, D the solute diffusivity in the liquid, k the partition coefficient and m the liquidus slope, which both slightly change with liquid composition (note that m is negative when $k < 1$), C_L the liquid composition between the grains which is unknown but varies between the nominal composition C_0 (20wt.%Cu) and the eutectic composition C_E (about 33wt.%Cu). In Fig. 5, the variations of the migration velocity as a function of the temperature gradient are plotted for three selected compositions in the expected range [20-33wt.%Cu]. The values of the different parameters used to draw the linear variations of TGZM velocity are given in Table 2. From Fig. 5, it can be concluded that there is a good agreement between the measured mean migration velocities and Tiller's model. This model predicts a linear increase of the TGZM migration velocity with the temperature gradient (Eq.1). This confirms that the global grain migration in the FoV is mainly due to the TGZM phenomenon. Unfortunately, it is not possible to estimate the composition of the liquid between the grains because of the large dispersion of measurements. This TGZM effect occurs for all

experiments but becomes negligible for larger cooling rates when it is hidden by the fast grain growth.

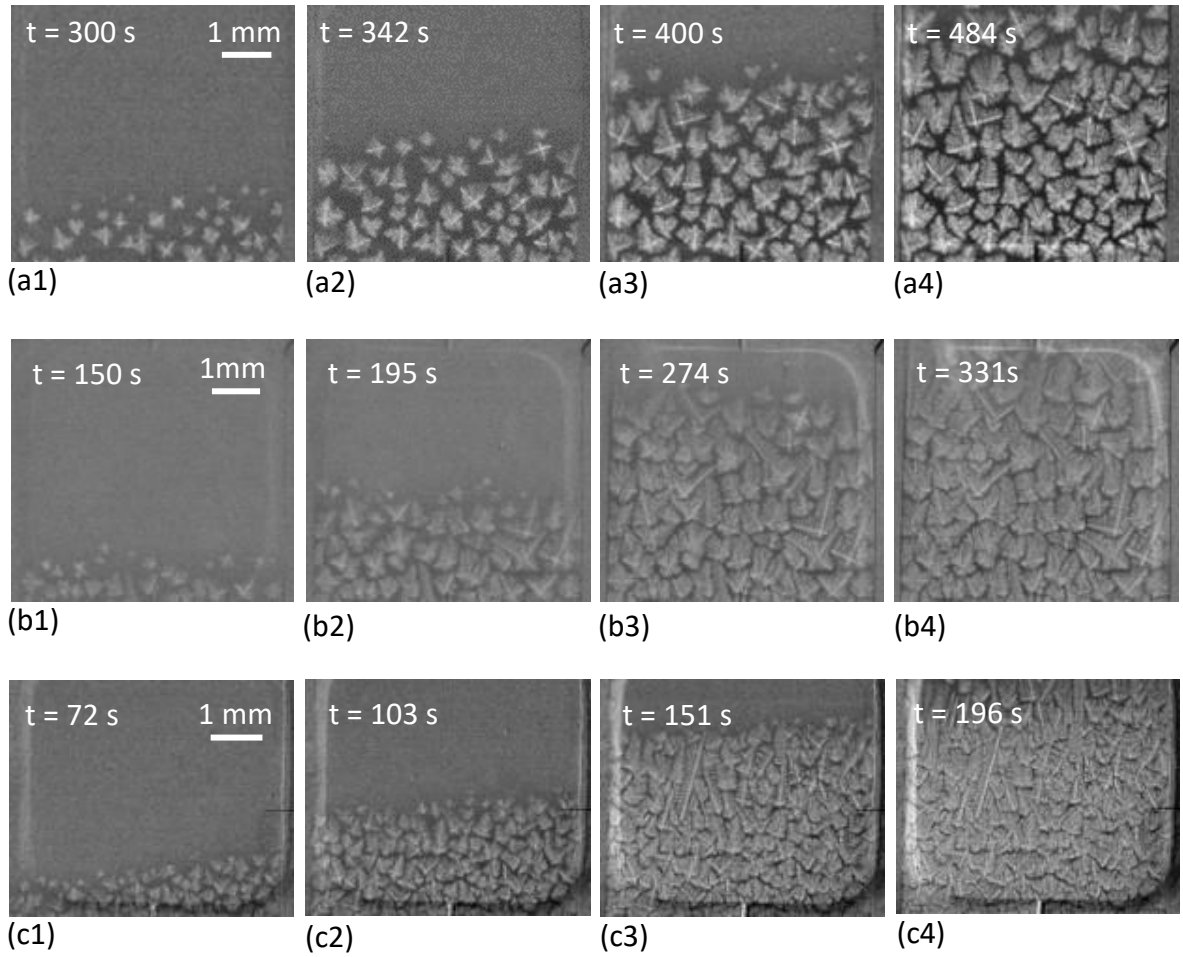

Fig. 4: Series of radiographs showing the propagation of refined Al - 20wt% Cu solidification front for three experiments carried out at intermediate growth velocity for increasing temperature gradient: (a) Experiment A2 (V_{mean} = 30.5 µm/s G_{mean} = 3.3 K/mm); (b) Experiment B2-2 (V_{mean} = 25.4 µm/s G_{mean} = 5.9 K/mm) and (c) Experiment C2 (V_{mean} = 32.2 µm/s G_{mean} = 9.3 K/mm).

Alloy composition	D (m^2/s)	m (K/wt.%Cu)	*k*
Al-20wt.%Cu	$3.5\ 10^{-9}$	-3.4	0.118
Al-25wt.%Cu	$3.5\ 10^{-9}$	-3.87	0.13
Al-30wt.%Cu	$3.5\ 10^{-9}$	-4.55	0.152

Table 2. Data used to calculate the variation of the grain migration velocities as a function of temperature gradient by equation (1). The given values are calculated by Thermocalc using the TTAL7 data base.

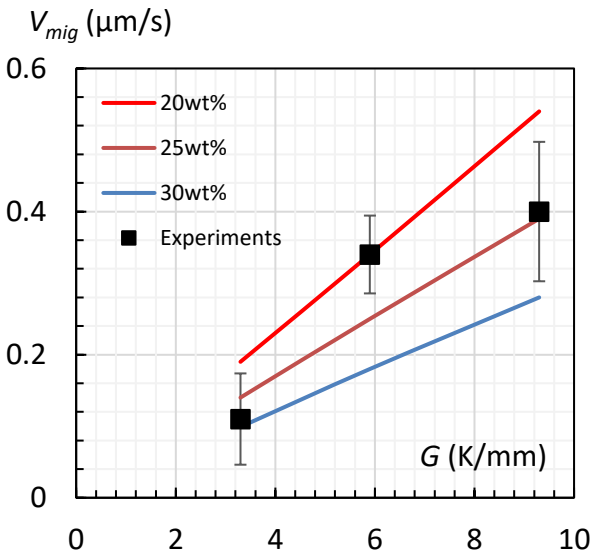

Fig.5: Variation of the Tiller's grain migration velocities (plain lines) by TGZM calculated for three values of liquid composition and experimental grain migration velocities (black squares) as a function of temperature gradient.

3.3. Impact of temperature gradient on nucleation distance

From the radiographs presented in Fig.4 (or the supplementary videos), the most striking observation was the difference of inter-dendritic liquid fraction between the three experiments, which can be seen with the naked eye. The higher the temperature gradient, the thinner the liquid channel between grains. This observation was valid for all experiments carried out at roughly the same average growth rate and increasing temperature gradients, enlightening an effect of the temperature gradient on the grain nucleation positions. To quantify this effect, we have performed the measurement of the nucleation distance $d_{n,}$ defined as the distance between the nucleation centre of a new grain and the dendrite tip of the nearest growing grain, as illustrated in Fig.6a that mimics a crop of a radiograph recorded during the experiment A2 performed at V_{mean} = 30.5 µm/s and G_{mean} = 3.3 K /mm (Fig.6b). It is worth noting that this type of measurement could only be done with the help of *in situ* observation during the nucleation phase and restricted to experiments at low or medium solidification rates due to spatial and time resolution limitations.

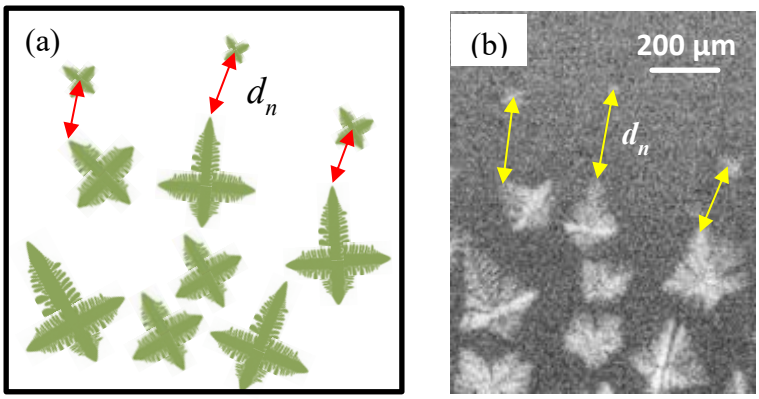

Fig. 6: (a) Sketch showing the nucleation distance d_n between grains. (b) Example of measured nucleation distances between the dendritic tip of an isolate grain and the centre of a grain which nucleated ahead it (experiment A2 with V_{mean} = 30.5 µm/s and G_{mean} = 3.3 K /mm).

The nucleation distance was determined for the four lowest velocities of each experiment series and the results are displayed in Fig. 7. Firstly, it can be seen that the nucleation distance decreases when the solidification velocity increases (from the blue top-curve to the black bottom-curve), which leads to a more homogeneous and finer grain structure, as discussed in [6]. Secondly, by comparing the experiments carried out with the same velocity and increasing temperature gradients, it was confirmed that the nucleation distance d_n decreases when the temperature gradient increases, regardless of the growth velocity. This is in line with the qualitative observation of radiographs (Fig.3 and Fig.4) showing a more compact grain structure for higher temperature gradients. Indeed, the decrease of the nucleation distance makes new grains nucleate closer to previous ones. Consequently, the amount of inter-dendritic liquid decreases between neighbouring grains. Finally, Fig.7 shows that the effect of the

temperature gradient on the nucleation distance gradually vanishes for larger growth velocities.

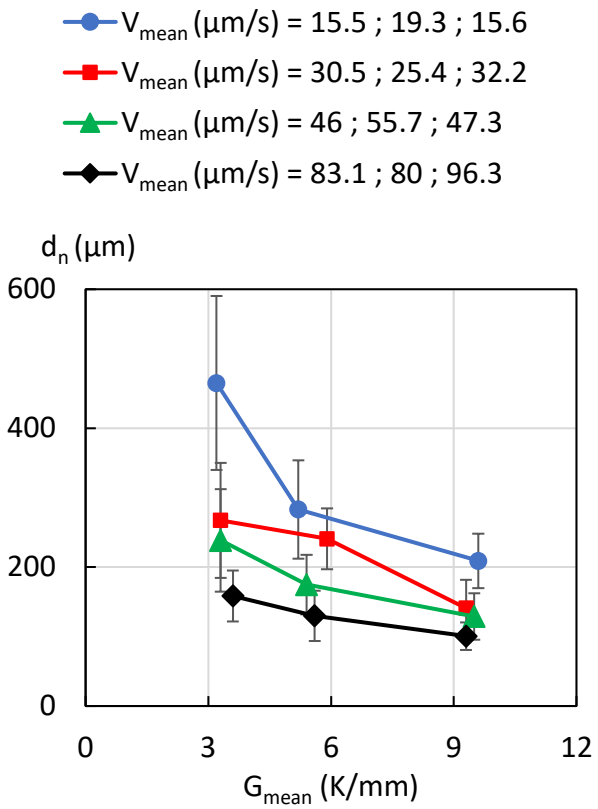

Fig. 7: Variation of nucleation distance as a function of temperature gradient, for different growth velocities during equiaxed growth of refined Al-20wt.% Cu alloys. In the top legend and for each series of symbols, the velocity values correspond to experiments for increasing temperature gradients.

The physical origin of this variation can be explained for instance by using the hemispherical model proposed by Kurz and Fisher [28]. Fig. 8 depicts the variation of the temperature in the liquid ahead of a hemispherical tip (black line), calculated for Al-20wt.%Cu at the same growth velocity V = 25 µm/s and two temperature gradients (a) G = 4 K/mm and (b) G = 6 K/mm. From these graphs, we can deduce that, while the maximum intensity of the

undercooling ΔT_{max} is relatively little affected, the length of the undercooled zone l_S decreases significantly with the increase of the temperature gradient. Consequently, the reduction in length of the undercooled zone explains why the grains nucleate closer and closer together at high temperature gradient, and then why the thickness of inter-dendritic liquid decreases. This explanation is in agreement with the concept of "Active Nucleation Zone" (ANZ) proposed by Xu *et al.* [7], which decreases with increasing temperature gradient.

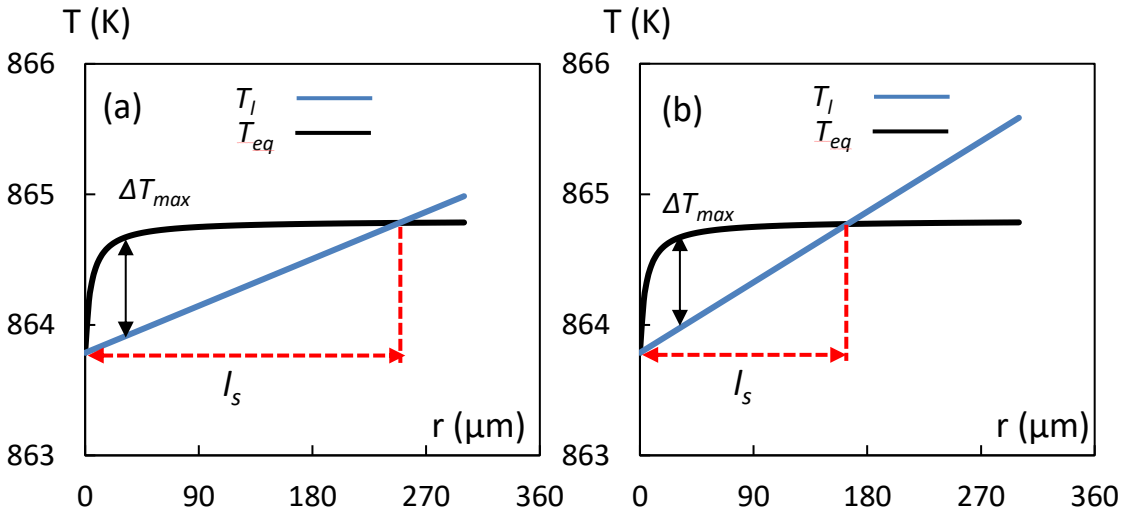

Fig. 8: Graphs showing the variation of the undercooled liquid zone in front of a hemispherical tip for Al-20wt%Cu at a fixed solidification velocity of V = 25 µm/s and a temperature gradient of (a) G = 4 K/mm and (b) G = 6 K/mm.

3.4. Variation of grain characteristic with increasing temperature gradient

The grain characteristics (diameter, elongation factor and growth orientation) are depicted in Fig.9 for the experiment C2, carried out with an intermediate nucleation front velocity V_{mean} = 32.2 µm/s and G_{mean} = 9.3 K/mm, which gives a typical equiaxed grain structure (Fig.9a). As

shown in [6, 22], the distribution of the grain diameter for all experiments is of gaussian-type (Fig.9b), meaning that an average grain size given by the maximum of the distribution (d_{peak} = *330* µm for this experiment*)* is selected. The grain diameter d distribution is related to the nucleation undercooling distribution which depends on the refiner particle size, as well as the interactions of each grain with its neighbours. For the present experiment and the others, the elongation factor ϕ distribution is well fitted by a log-normal curve, which pointed out an asymmetry of this parameter (Fig.9c). Most grains have an elongation factor ranging from 1.2 (nearly equiaxed grains) to 3 (short elongated grains), while a very few grains had an elongation factor larger than three. This type of grain structure could be considered as "equiaxed" according to Hunt's criterion [20], although it was formed in a temperature gradient. The non-isothermal conditions prevents to obtain a perfect equiaxed grains structure and explain the value of 1.2 of the lower limit of the elongation factor as discussed in [6]. Finally, the grain growth orientation θ distribution of the C2 experiment is of gaussian-type, with a peak around zero which is the temperature gradient direction (Fig.9d). For higher growth velocities, the orientation distributions become flatter and flatter, showing a tendency of a randomly orientation of grains, as expected for an equiaxed microstructure, which means that equiaxed grain growth direction is lesser and lesser influenced by the temperature gradient.

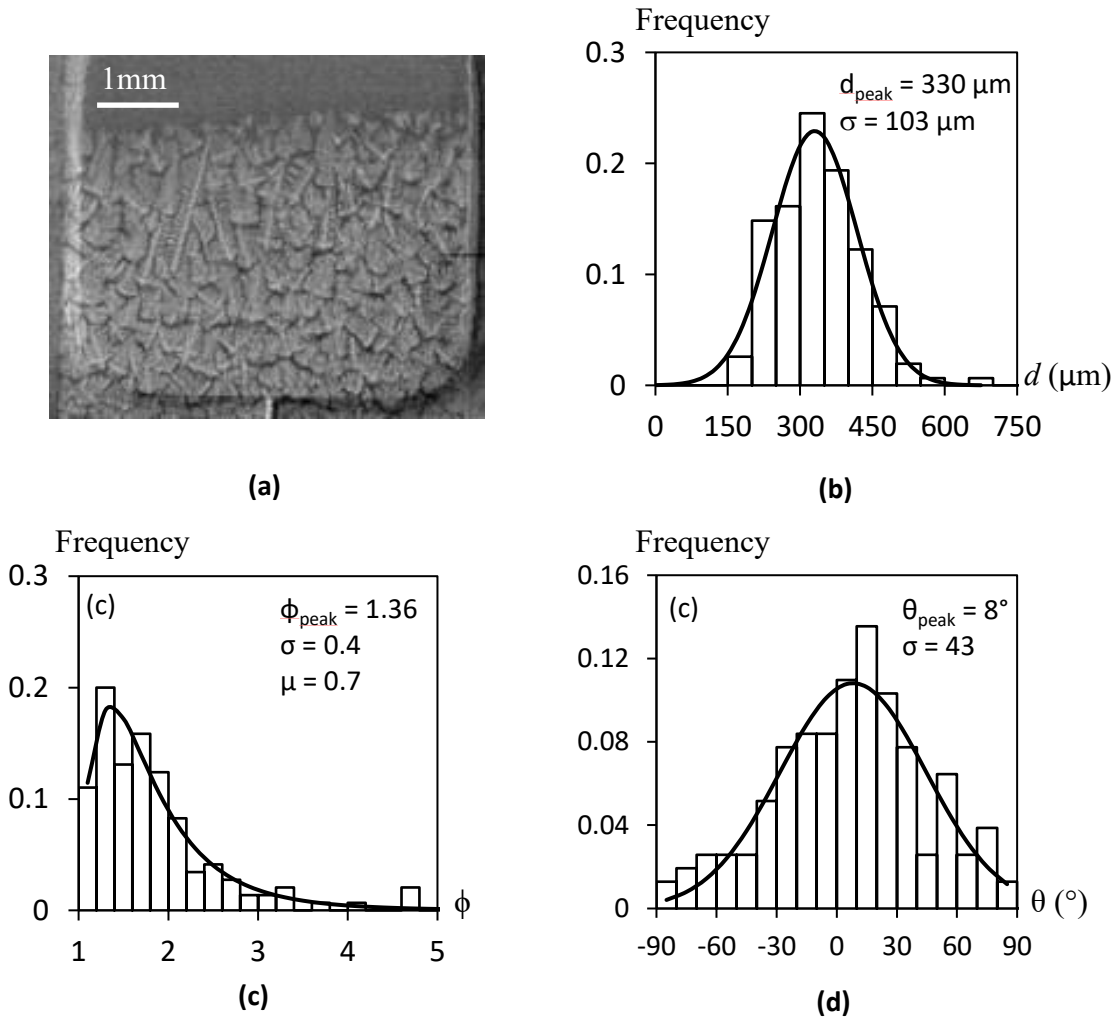

Fig. 9: Experiment C2, directional solidification of refined Al-20wt.%Cu alloy carried out at V_{mean} = 32.2 µm/s and a temperature gradient G_{mean} = 9.3 K/mm. (a) Radiograph showing the grain structure of C2 experiment; (b) Distribution of the grain diameter d; (c) Distribution of the elongation factor ϕ; (d) Distribution of the growth orientation θ.

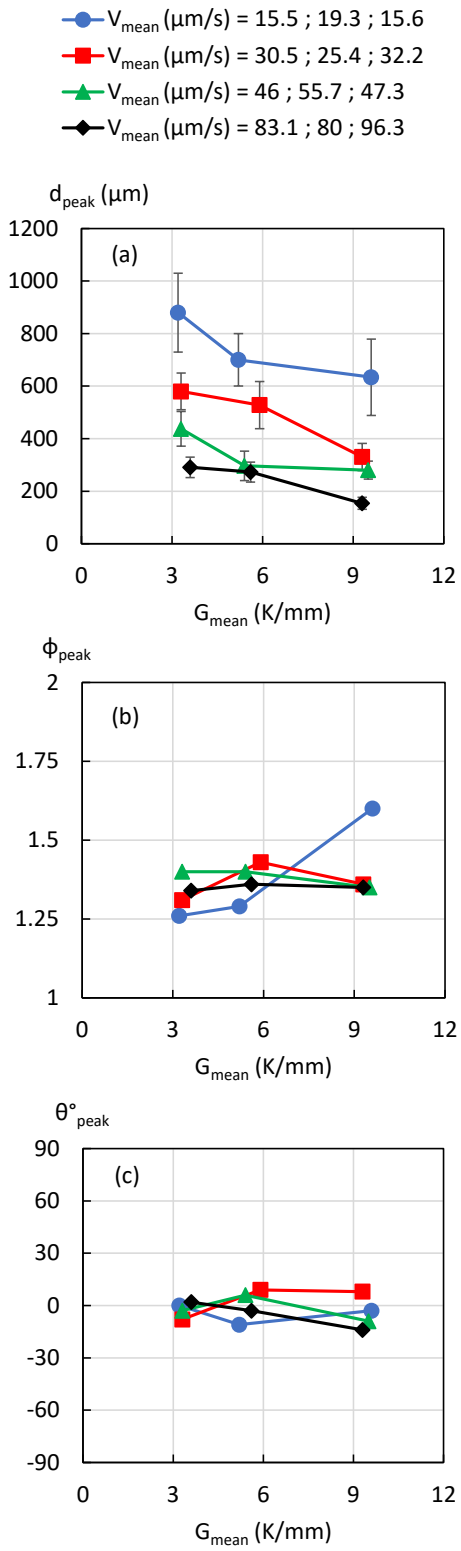

Fig.10: (a) Variation of the grain size as a function of the temperature gradient for four series of experiments; (b) Variation of the grain elongation for four series of experiments and (c) Variation of the grain growth orientation for four series of experiments. In the top legend and

for each series of symbols, the velocity values correspond to experiments for increasing temperature gradients.

The impact of the temperature gradient on the three grain characteristics is enlighten in Fig.10. Fig. 10a shows the variation of the average or maximum grain size d_{peak} as a function of the temperature gradient G_{mean} for the four growth velocities. From the curves, it can be concluded that the grain size decreases not only with the increase of growth velocity (from the blue top-curve to the black bottom-curve) as reported in [6] but also with the increase of the temperature gradient. The physical origin of grain size reduction with temperature gradient can be ascribed to the simultaneous decrease of the maximum undercooling and the solutal length as drawn in Fig.8. Indeed, the decrease of the solutal length reduces the nucleation distance and thus gives a more compact grain structure. The very close nucleation of a new grain layer will stop rapidly the growth of the existing layer and thus reduce the average grain size. This feature perfectly fits with what one can see in Fig.4, as well as all other series of experiments. This variation of the grain size with the temperature gradient was predicted numerically by Badillo and Beckermann [29] using 2D phase-field approach. As in the present experiments, the authors evidenced that the equiaxed grains are quite elongated for the lowest temperature gradient, and more refiners are activated when increasing the temperature gradient. The authors also found that, beyond a critical value of the temperature gradient, a fully columnar microstructure is achieved in agreement with the Hunt's columnar-equiaxed map and all experiment observations. Vandyoussefi *et al.* [5] applied "cellular automaton – finite element (CA-FE)" simulations to

study the influence of the temperature gradient on the final grain structure for Al-4.15wt% Mg alloys. At constant growth velocity and density of nucleation events, the simulations also predict that increased temperature gradient gives finer, but more elongated, grains.

The variation of grain morphology, in particular the grain elongation, is illustrated by Fig.10b. For a sake of legibility, error bars are not drawn in Fig.10b because almost the same value was measured for all experiments ± 0.3. For all experiments the peak in grain elongation factor ϕ_{peak} is lower than two, which means that the grains are of equiaxed type, according to Hunt's criterion [20]. For the three high growth velocities (V = 30 µm/s, 50 µm/s and 86 µm/s), the average grain elongation factors are roughly constant, and no effect of G is detectable. The average values for those three high velocity experiments are higher to unity, which shows that the grains are not perfectly equiaxed due to the temperature gradient influence. As mentioned in [6, 7], the existence of a temperature gradient promotes a preferential growth of grains along temperature gradient direction that is confirmed by the measurements of the orientation angle θ_{peak} of the grain (Fig.10c). For all experiment, the orientation growth of grains is around zero, which is the temperature gradient direction.

The influence of temperature gradient on grain elongation factor is only significant for the lowest growth velocity (blue curve in Fig.10b), when the peak in grain elongation factor ϕ_{peak} rises with increasing temperature gradient, which indicates that the grain shape evolves from "nearly equiaxed grains" ($\phi = 1.25$) to more "elongated grains" ($\phi = 1.6$), as also visible in Fig.3.

It is worth mentioning that our experimental observations for the grain size evolution are

contrary to the ones reported in Xu *et al.* [7] in the same alloy but with a different refiner composition and amount (0.05 wt.% Al-5Ti-1B). These different behaviours could be attributed to the fact that the increase of the temperature gradient has two opposite effects. On one hand, increasing G leads to a reduction of the undercooled liquid zone length l_s as drawn in Fig.8, which promotes the nucleation of new grains closer to the tip of the existing dendrite and thus reduces the average grain size as displayed in Fig.10a. Increasing G also favours the growth of existing dendrite grains in the heat flux direction, which gives more elongated grains. On the other hand, increasing G also leads to a reduction of the liquid undercooling intensity (Fig.8) and then of the number of activated refiners. Thus, the impact of the temperature gradient may be different depending on the refiner composition and size distribution. Further systematic investigations would be necessary to enlighten the respective impact of refiner composition, size distribution and amount on the grain size evolution with the temperature gradient.

The present observations are in agreement with the CAFE simulations of Vandyoussefi *et al.* [5] who showed that at constant V and maximum possible density of nucleation events N_{max}, the grains become smaller and progressively elongated as G rises. The similarity of the trend with the experimental observations suggests that the present composition of the refiner provides enough active particles to induce the same change of the grain structure. It also confirms the fact that grain size and morphology are the result of the competition between grain nucleation and grain growth in the temperature gradient direction.

4. Conclusion

Directional solidification of refined Al-20wt.%Cu samples was studied using X-radiography generated by the SFINX laboratory device to analyse the impact of the temperature gradient on the dynamic of the equiaxed grain structure formation. Quantitative information on the dynamic of grain structure formation (TGZM and nucleation distance), as well as the final size, shape and orientation of grains were obtained as a function of temperature gradient variation.

The results showed that the grain migration velocities due to the TGZM phenomenon is more significant at high temperature gradient and low growth velocity, which is consistent with Tiller's model. Analysis of the radiographs shows that the nucleation distance decreases with the increase of temperature gradient, which means that grains nucleate closer to the tip of the existing dendrites. This effect reduces the grain size because the very close nucleation of a new grain layer will stop the growth of the previously existing layer. Measurements also show that a high temperature gradient results in more elongated and more oriented grains at low growth velocity. For high growth velocities, it has been found no significant effect of the temperature gradient in our experiments. The current results present an original set of data that can be used for models and numerical simulations.

5. Acknowledgements

This work is supported by the XRMON project (AO-2004-046) of the MAP program of the European Space Agency (ESA), by the French National Space Agency (CNES) and the French-Algerian doctoral fellowship program PROFAS B+. The authors would also like to thank the Swedish Space Corporation (SSC) for the development of the SFINX facility and the technical support.

6. References

[1] E.O. Hall, The Deformation and Ageing of Mild Steel: II Characteristics of the Lüders Deformation, Proceedings of the Physical Society. Section B, London, B 64 (1951) 742-747.

[2] N. J. Petch, The Cleavage Strength of Polycrystals, Journal of the Iron and Steel Institute, 174 (1953) 25-28.

[3] W. Kurz, D.J. Fisher, R. Trivedi, Progress in modelling solidification microstructures in metals and alloys: dendrites and cells from 1700 to 2000, International Materials Reviews, 64 (2019) 311-354.

[4] W. Kurz, M. Rappaz, R. Trivedi, Progress in modelling solidification microstructures in metals and alloys. Part II: dendrites from 2001 to 2018, International Materials Reviews, (2020) 1-47.

[5] M. Vandyoussefi, A.L. Greer, Application of cellular automaton-finite element model to the grain refinement of directionally solidificed Al-4.15wt%Mg alloys, Acta Materiala, 50 (2002) 1693-1705.

[6] H. Soltani, G. Reinhart, M.C. Benoudia, F. Ngomesse, M. Zahzouh, H. Nguyen-Thi, Impact of growth velocity on grain structure formation during directional solidification of a refined Al-20 wt.%Cu alloy, Journal of Crystal Growth, 548 (2020) 125819.

[7] Y.J. Xu, D. Casari, R.H. Mathiesen, Y.J. Li, Revealing the heterogeneous nucleation behavior of equiaxed grains of inoculated Al alloys during directional solidification, Acta Materialia, 149 (2018) 312-325.

[8] Y. Jia, D. Wang, Y. Fu, A. Dong, G. Zhu, D. Shu, B. Sun, In situ Investigation of the Heterogeneous Nucleation Sequence in Al-15 Weight Percent Cu Alloy Inoculated by Al-Ti-B, Metallurgical and Materials Transactions A, 50 (2019) 1795-1804.

[9] R.H. Mathiesen, L. Arnberg, H. Nguyen-Thi, B. Billia, In Situ X-Ray Video Microscopy as a Tool in Solidification Science, JOM, 64 (2012) 76-82.

[10] H. Nguyen-Thi, L. Salvo, R.H. Mathiesen, L. Arnberg, B. Billia, M. Suery, G. Reinhart, On the interest of synchrotron X-ray imaging for the study of solidification in metallic alloys, Comptes Rendus Physique, 13 (2012) 237-245.

[11] H. Nguyen-Thi, G. Reinhart, G.S. Abou Jaoude, R.H. Mathiesen, G. Zimmermann, Y. Houltz, D. Voss, A. Verga, D.J. Browne, A.G. Murphy, XRMON-GF: A novel facility for solidification of metallic alloys with in situ and time-resolved X-ray radiographic characterization in microgravity conditions, Journal of Crystal Growth, 374 (2013) 23-30.

[12] C. Rakete, C. Baumbach, A. Goldschmidt, D. Samberg, C.G. Schroer, F. Breede, C. Stenzel, G. Zimmermann, C. Pickmann, Y. Houltz, C. Lockowandt, O. Svenonius, P. Wiklund, R.H. Mathiesen, Compact x-ray microradiograph for in situ imaging of solidification processes: Bringing in situ x-ray micro-imaging from the synchrotron to the laboratory, Review of Scientific Instruments, 82 (2011).

[13] A. Bogno, H. Nguyen-Thi, B. Billia, G. Reinhart, N. Mangelinck-Noel, N. Bergeon, T. Schenk, J. Baruchel, In situ and real-time analysis of the growth and interaction of equiaxed grains by synchrotron X- ray radiography, in: 3rd International Conference on Advances in Solidification Processes, IOP Publishing Ltd, Bristol, 2012.

[14] A. Bogno, H. Nguyen-Thi, A. Buffet, G. Reinhart, B. Billia, N. Mangelinck-Noël, N. Bergeon, J. Baruchel, T. Schenk, Analysis by synchrotron X-ray radiography of convection effects on the dynamic evolution of the solid-liquid interface and on solute distribution during the initial transient of solidification, Acta Materialia, 59 (2011) 4356-4365.

[15] A.G. Murphy, R.H. Mathiesen, Y. Houltz, J. Li, C. Lockowandt, K. Henriksson, G. Zimmermann, N. Melville, D.J.

Browne, XRMON-SOL: Isothermal equiaxed solidification of a grain refined Al–20 wt%Cu alloy, Journal of Crystal Growth, 440 (2016) 38-46.
[16] S. Akamatsu, H. Nguyen-Thi, In situ observation of solidification patterns in diffusive conditions, Acta Materialia, 108 (2016) 325-346.
[17] H. Nguyen-Thi, G. Reinhart, B. Billia, On the interest of microgravity experimentation for studying convective effects during the directional solidification of metal alloys, Comptes Rendus Mécanique, 345 (2017) 66-77.
[18] A. Bogno, G. Reinhart, A. Buffet, H. Nguyen Thi, B. Billia, T. Schenk, N. Mangelinck-Noël, N. Bergeon, J. Baruchel, In situ analysis of the influence of convection during the initial transient of planar solidification, Journal of Crystal Growth, 318 (2011) 1134-1138.
[19] M. Abramoff, P. Magalhães, S.J. Ram, Image Processing with ImageJ, Biophotonics International, 11 (2003) 36-42.
[20] J.D. Hunt, Steady State Columnar and Equiaxed Growth of Dendrites and Eutectic, Materials Science and Engineering, 65 (1984) 75-83.
[21] Y.Z. Li, N. Mangelinck-Noël, G. Zimmermann, L. Sturz, H. Nguyen-Thi, Comparative study of directional solidification of Al-7 wt% Si alloys in Space and on Earth: Effects of gravity on dendrite growth and Columnar-to-equiaxed transition, Journal of Crystal Growth, 513 (2019) 20-29.
[22] H. Soltani, F. Ngomesse, G. Reinhart, M.C. Benoudia, M. Zahzouh, H. Nguyen-Thi, Impact of gravity on directional solidification of refined Al-20wt.%Cu alloy investigated by in situ X-radiography, Journal of Alloys and Compounds, 862 (2021) 158028.
[23] A. Prasad, S.D. McDonald, H. Yasuda, K. Nogita, D.H. StJohn, A real-time synchrotron X-ray study of primary phase nucleation and formation in hypoeutectic Al–Si alloys, Journal of Crystal Growth, 430 (2015) 122-137.
[24] H. Nguyen-Thi, G. Reinhart, N. Mangelinck-Noël, H. Jung, B. Billia, T. Schenk, J. Gastaldi, J. Härtwig, J. Baruchel, In-Situ and Real-Time Investigation of Columnar-to-Equiaxed Transition in Metallic Alloy, Metallurgical and Materials Transactions A, 38 (2007) 1458-1464.
[25] H. Nguyen-Thi, G. Reinhart, A. Buffet, T. Schenk, N. Mangelinck, H. Jung, N. Bergeon, B. Billia, H. Härtwig, J. Baruchel, In situ and Real-time analysis of TGZM phenomena by synchrotron X-ray radiography, Journal of Crystal Growth, 310 (2008) 2906-2914.
[26] H. Nguyen Thi, B. Drevet, J.M. Debierre, D. Camel, Y. Dabo, B. Billia, Preparation of the Initial Solid - Liquid Interface and Melt in Directional Solidification, Journal of Crystal Growth, 253 (2003) 539-548.
[27] W.A. Tiller, Migration of liquid zone through a solid: Part I, Journal of Applied Physics, 34, 9 (1963) 2757.
[28] W. Kurz, D.J. Fisher, Fundamentals of Solidification, Trans Tech Publications ltd, , 1998.
[29] A. Badillo, C. Beckermann, Phase-field simulation of the columnar-to-equiaxed transition in alloy solidification, Acta Materialia, 54 (2006) 2015-2026.